Journal of Hydroscience and Hydraulic Engineering
Vol. 2, No. 1, April, 1984, pp.27-45.

CHARACTERISTICS OF FLOW AND TURBULENCE NEAR INTERFACIAL WAVES IN UPPER-LAYER FLOW

By

Masaru Ura,

Department of Civil Engineering, Kyushu Institute of Technology,
Tobata-ku, Kitakyushu 804, Japan

Toichiro Tsubaki and Nobuhiro Matsunaga

Department of Civil Engineering Hydraulics and Soil Mechanics,
Kyushu University, Fukuoka 812, Japan

SYNOPSIS

The characteristics of mean velocity profiles, velocity fluctuations and interfacial fluctuations in two-layered flows have been investigated using two components of velocity and interfacial displacements measured simultaneously. Experimental results are expressed consistently in non-dimensional forms composed of the interfacial physical quantities. Interfacial fluctuations consist of a long periods (L.P. wave) and short periods (S.P. wave), and induce a pair of vortical flows of the cat's eye pattern corresponding to the L.P. and S.P. waves. Based on the vertical profiles of the intensities of fluctuating velocities, it is made clear that the velocity fluctuations close to the interface are induced mainly by wave motion and vortical organized motion. The mean velocity profiles in the lower layer are analized by introducing an effective viscosity. The coefficient of interfacial friction is predictable as a function of the Iwasaki number.

INTRODUCTION

It is important in hydraulic engineering to estimate the shear stress acting on an interface of two-layered density currents and the velocity of entrainment. They depend closely on the characteristics of turbulent shear flows and interfacial fluctuations. Many experimental investigations (1, 4, 14, 16, 19) on the behavior of the interfacial fluctuations have been carried out in upper-layer flows. It has been widely recognized that they have two kinds of predominant waves. One wave propagates faster in the down-stream direction than fluid particles at the interface, and has a wave profile with a steep crest and a flat trough. The other has a flat crest and a steep trough and its phase velocity is slower than the interfacial fluid velocity. The former has a higher frequency than the latter. One (16, 18) of the authors has called them 'short period wave' and 'long period wave'. Andow, Hanawa and Toba (1) has called them 'positive wave' and 'negative wave', and observed vortical flows of the cat's eye pattern induced above the positive wave and below the negative wave by means of flow visualization. Recently, Nishida and Yoshida (15) have shown that two kinds of unstable waves form based on the stability analysis of shear flow with a hyperbolic velocity distribution.

As to the characteristics of flow and turbulence in upper-layer flow, Tsubaki, Komatsu and Shimoda (18) have made a series of experiments in connection with interfacial waves. Hino, Nguyen and Nakamura (5) have studied the microstructure of flow field visualized with hydrogen-bubbles. Hino and Nguyen (6) have obtained a vertical distribution of mean velocity using the Monin-Obukhov similarity analysis for a diabatic atmospheric boundary layer, and have estimated theoretically

the interfacial friction coefficient.

On the other hand, only a few experimental studies on lower-layer flow have been made; e.g. Lofquist's study (13) on mean flow and recent studies by Kato et al. (9,10) on turbulence and entrainment. Introducing an effective viscosity instead of the kinematic viscosity, Csanady (2) examined in detail the characteristics of velocity profile non-dimensionalized by the interfacial shear velocity.

Although a lot of information on the upper-layer flow has been obtained as mentioned above, scarce are experimental investigations carried out for the purpose of estimating characteristic quantities related to mean velocity profiles and fluctuations of velocity and interface on the basis of local, leading parameters.

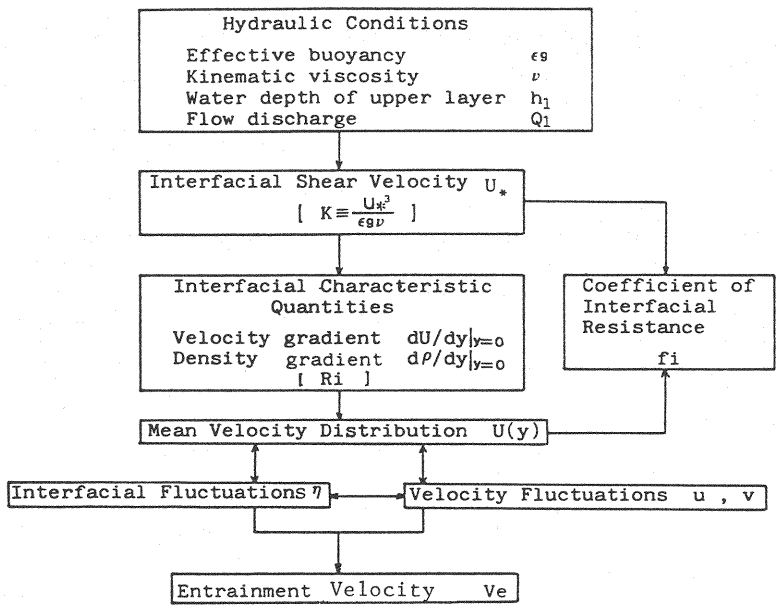

Fig. 1 Main process of characteristic quantities forming in two-layered flow field.

Fig. 1 shows main process of the characteristic quantities forming in two-layer flow. The process, in which complicate interactions between the quantities are not considered, is explained as follows. First, the interfacial shear velocity U_* is determined uniquely after the hydraulic conditions are given, and the interfacial Keulegan parameter $K\ (=U_*^3/\varepsilon g\nu)$ is introduced as an important non-dimensional parameter. Second, the velocity and density gradients at the interface are determined by the hydraulic conditions and U_*. As another non-dimensional parameter, the interfacial Richardson number Ri is derived. Third, a vertical profile of the mean velocity close to the interface is established on the basis of the gradients, and velocity and interfacial fluctuations are generated in equilibrium with the flow field. Fourth and last, the entrainment velocity which is dominated directly by the fluctuations is determined. The coefficient f_i of interfacial friction is obtained from the mean velocity profile and U_*.

The main purposes of this paper are (i) to estimate the characteristic quantities universally and consistently by using either K or Ri as an interfacial parameter through experiments on upper-layer flow, (ii) to understand the interaction between the velocity and interfacial fluctuations, and (iii) to present a simulation model on the interfacial friction coefficient. Experimental results will be discussed along with the process shown in Fig. 1.

EXPERIMENTAL METHODS

Experiments were carried out by using a flume illustrated in Fig. 2. The flume was 6.0 m long, 0.3 m deep and 0.26 m wide, and had a horizontal bottom and transparent, acrylic side walls. Fresh water was used as a working fluid of upper layer and salt water as that of lower layer. The fluids were supplied into the flume from constant head tanks. Especially, the salt water was oozed uniformly along the flume through a porous pipe equipped on the bottom. A rigid guiding plate with 1 m length was attached horizontally at the upstream end of the flume and at 0.15 m elevation from the bottom in order to avoid undesirable strong mixing between the fluids. On the other hand, the following devices were considered at the downstream end. The fresh water was overflowed to keep a water level constant. In order to avoid the reflection of interfacial waves and the development of a layer with intermediate density, the fluid in the neighborhood of an interface was drained at the downstream end through an outlet so that the flow field in the test section was not disturbed.

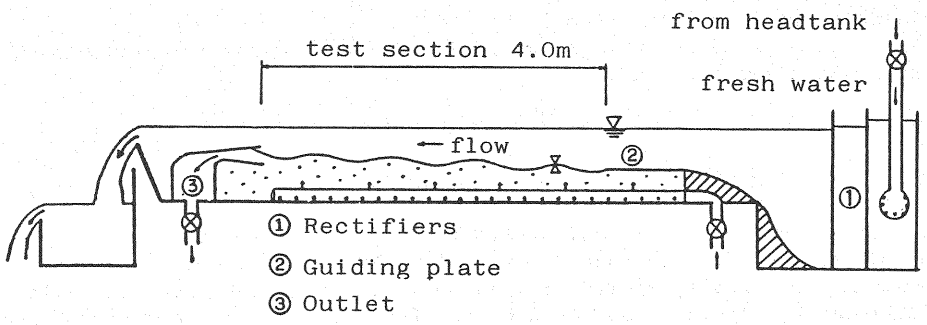

Fig. 2 Experimental flume.

Two-layered density currents were set up by letting a constant volume of the fresh water flow on the salt water stored previously in the flume. The discharge of the salt water was controlled so that the position of the interface was coincided with that of the guiding plate at the upstream end and the mean depth h_2 and density ρ_2 of the lower layer were kept constant. Tap water was also supplied in a fresh water tank to avoid the increase of density ρ_1 of the upper layer. The mean flow field was made steady by such adjustments.

Two components of fluid velocity, salinity concentration of the fluids and interfacial displacements were measured simultaneously by using a V-shaped hot-film velocity probe, a four-pole electric conductivity probe and two resistance-type wave gauges, respectively. The velocity probe was attached to the lower end of a point gauge movable along a vertical line. The conductivity probe was fixed to the velocity probe at a horizontal interval of 0.5 cm to measure at the almost same position. The wave gauges were placed at a 1.0 cm interval to obtain phase velocities of the interfacial fluctuations. The phase velocities were calculated by using phase lags between interfacial displacements measured at the two points: the phase lags were estimated from co- and quadrature-spectra of the displacements. The three sensors, i.e. the wave gauge in the upstream side and the probes of velocity and conductivity, were set in a plane perpendicular to the flow direction. Signals obtained at each measuring point were recorded for four minutes on a data recorder. The signals were digitized; the sampling time and the number of the sampling were 1/18.75 sec and 4096, respectively. The density of the fluids were calculated from the salinity concentration.

A procedure of measurement was as follows. After the flow field became steady, the mean level of the interface was measured at 0.25 m intervals in the downstream direction from the edge of the guiding plate, and the slope of the interface from the horizontal was obtained. The interface was defined as a position where the mean density was $(\rho_1 + \rho_2)/2$, and its mean level was determined by monitoring time

series of the salinity concentration close to the interface in a pen-recorder. The probes and gauges were set at the middle of a region where the slope was uniform, i.e. about 2.75 m downstream of the edge of the guiding plate. Vertical profiles of the fluid velocity and density were obtained by moving the point gauge while the wave gauges remained at the interface.

Twenty-three runs were tested out by varying the non-dimensional density effect ϵ defined by $(\rho_2 - \rho_1)/\rho_2$, the kinematic viscosity ν of the working fluids, the depth h_1 of the upper layer and the velocity Um averaged over a cross section of the upper layer. The ranges of the hydraulic conditions and overall non-dimensional parameters are summarized in Table 1, where $Fr = Um/\sqrt{\epsilon g h_1}$ = internal Froude number; $Re = Um h_1/\nu$ = Reynolds number; and $\Psi = Um^3/\epsilon g \nu$ = Iwasaki number (6).

Table 1 Ranges of hydraulic conditions and overall parameters.

Symbol	Range
$\epsilon \times 10^3$	3.0 ~ 22.7
$\nu \times 10^2$ (cm²/s)	0.883 ~ 1.28
h_1 (cm)	5.90 ~ 10.00
Um (cm/s)	1.05 ~ 7.38
$Fr = Um/\sqrt{\epsilon g h_1}$	0.152 ~ 0.651
$Re = Um h_1/\nu$	640 ~ 4940
$\Psi = Um^3/\epsilon g \nu$	14.8 ~ 2090

MEAN FLOW PROPERTIES

Definition of Profiles of Mean Velocity and Density

A schematic diagram of vertical profiles of the mean velocity U(y) and density $\rho(y)$ in an upper-layer flow is shown in Fig. 3. The coordinate axis x is taken downstream, and y vertically upward from the mean level of the interface. In the figure, the mean flow field is subdivided into five regions on the basis of the flow properties and notations of characteristic quantities are described. The depth of the upper layer is represented by h_1 and that of the lower layer by h_2. The distances h_1' and h_2' denote those from the interface to the position where U(y) begins to become a uniform velocity U_1 and to the first position of U(y) = 0, respectively. The distances Δ_1 and Δ_2 will be determined later on the basis of non-dimensional vertical profiles of the mean velocity and the intensities of fluctuating velocities. The mean velocity at the interface is indicated by Ui. Length scales δ_m and δ_ρ are defined as the equations

$$\delta_m = Um/\left(\frac{dU}{dy}\right)_{y=0}$$

$$\delta_\rho = (\rho_2 - \rho_1)/\left|\frac{d\rho}{dy}\right|_{y=0}$$

where $(dU/dy)_{y=0}$, $(d\rho/dy)_{y=0}$ = gradients of the mean velocity and density at the interface.

Region ① in the range of $h_1' \leq y \leq h_1$ is called '*uniform flow layer*'. Region ② is the range of $\Delta_1 \leq y \leq h_1'$ and is called '*turbulent shear layer*' where the buoyancy effect seems to be negligible and the velocity fluctuations induced by shear flow are dominant. Region ③ is the range of $-\Delta_2 \leq y \leq \Delta_1$ and is called '*interfacial layer*'. In this region, the buoyancy effect

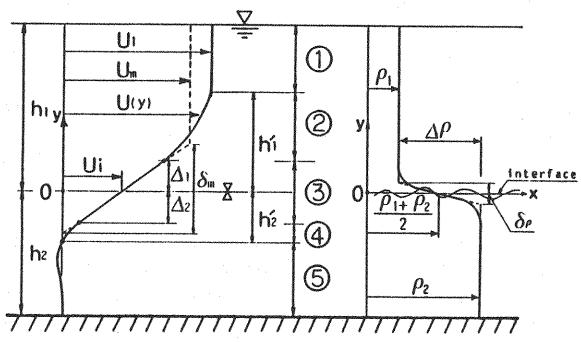

Fig. 3 Definition of characteristic quantities related to mean velocity and density.
① Uniform flow layer,
② Turbulent shear layer,
③ Interfacial layer,
④ Quasi-viscous layer,
⑤ Return flow layer.

becomes important and the velocity fluctuations are induced by wave motion and vortical organized motion such as flow of the cat's eye pattern. Region ④, in which the effect of fluid viscosity is important though there is some influence of the vortical motion, is the range of $-h_2' \leq y \leq -\Delta_2$ and is called '*quasi-viscous layer*'. Region ⑤ is the range of $y \leq -h_2'$ and is called '*return flow layer*'.

Interfacial Shear Velocity and Effective Viscosity

It was tried to evaluate the interfacial shear velocity U_* using the equation

$$U_* = \sqrt{-\overline{uv} + \nu \frac{dU}{dy}\Big|_{y=0}}$$

where $-\rho_1 \overline{uv}$ = Reynolds stress. However, the accurate evaluation was difficult since the values of $-\overline{uv}$ scattered near the interface owing to the interfacial fluctuations. In this paper, therefore, U_* is estimated from the equation

$$U_* = \sqrt{-\varepsilon g h_1 \frac{dh_1}{dx}(1 - Fr^2)\frac{h - h_1}{h} - 2\frac{\tau_W}{\rho_1}\frac{h_1(h - h_1)}{Bh}} \qquad (1)$$

which is derived from a non-uniform flow model of two-layered density currents; h = total water depth; B = width of the flume; and τ_W = shear stress acting on a side wall. The shear stress τ_W is given by

$$\frac{\tau_W}{\rho_1} = 0.055\left(\frac{Um\,B}{2\nu}\right)^{-1/4}\frac{Um^2}{2}$$

if the Blasius law of resistance is adopted.

Csanady introduced an effective viscosity ν_e defined by $U_*^2/\left(\frac{dU}{dy}\right)_{y=0}$ and showed that ν_e/ν for lower-layer flow is expressed by $7.3\,K^{1/2}$ using Lofquist's data. Moreover, he confirmed the validity of the $K^{1/2}$-dependence of ν_e/ν by considering the existence of interfacial waves. In Fig. 4 the values of ν_e/ν based on the present experimental results are plotted against K together with Csanady's results. The values of ν_e/ν in the upper-layer flow is also proportional to $K^{1/2}$ though they are slightly smaller than Csanady's results. As interfacial displacements and fluctuating velocities at the interface become small with decrease of K, ν_e approaches to ν. Therefore, the equation

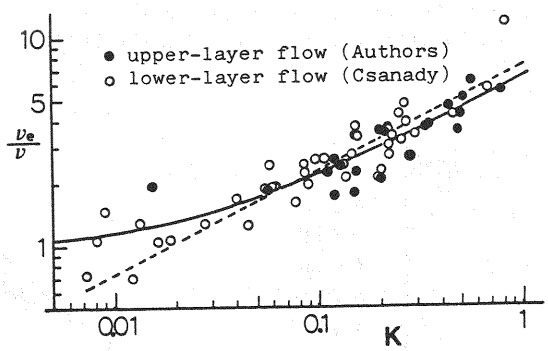

Fig. 4 K-dependence of ν_e/ν.
The broken line indicates $\nu_e/\nu = 7.3K^{1/2}$ and the solid line Eq. 2 .

$$\nu_e/\nu = (1 + 40K)^{1/2} \qquad (2)$$

is given as an empirical formula for the upper- and lower-layer flows.

Mean Velocity Profile for Upper Layer

Fig. 5 shows $(U-Ui)/U_*$ plotted against $|y|/\delta_*$, where δ_* is defined by

$$\delta_* = U_* / (\frac{dU}{dy})_{y=0} = \nu_e / U_*$$

The broken line indicates the velocity distribution derived from the wall law applicable to turbulent shear flows close to a smooth rigid wall. As will be obvious from the figure, a linear profile

$$\frac{U - Ui}{U_*} = \frac{y}{\delta_*} \qquad (3)$$

holds in the range of $y/\delta_* \lesssim 4 \sim 6$. The upper limit of the interfacial layer is determined empirically by $\Delta_1 = 4\delta_* \sim 6\delta_*$. In the turbulent shear layer, the velocity distribution has a logarithmic profile and is expressed by

$$\frac{U - Ui}{U_*} = \frac{1}{\kappa} \ln \frac{y}{\Delta_1} + \frac{\Delta_1}{\delta_*} \qquad (4)$$

where κ = von Kármán constant (assumed to be 0.4). As $U=U_1$ in the uniform layer, the equation

$$\frac{U_1 - Ui}{U_*} = \frac{1}{\kappa} \ln \frac{h_1'}{\Delta_1} + \frac{\Delta_1}{\delta_*} \qquad (5)$$

is obtained. If ν_e is used instead of ν, the velocity distribution in the upper-layer flow is described analogously to that of wall-bounded turbulent shear flow. The values of Δ_1/δ_* seem to increase slightly as Ψ increases, but h_1'/δ_* increase distinctly. The velocity distribution in the lower layer will be discussed in the section of INTERFACIAL FRICTION COEFFICIENT.

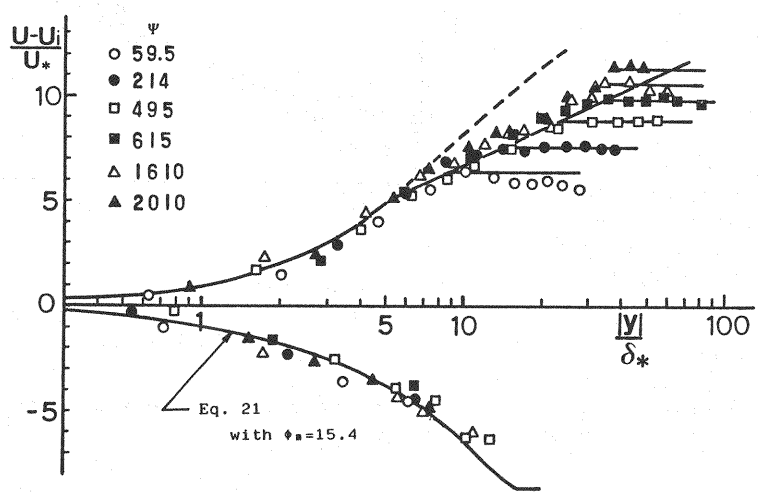

Fig. 5 Vertical distribution of mean velocities.

INTERFACIAL FLUCTUATIONS

It has been observed that interfacial fluctuations consist of two types of waves and found that phase velocities of the waves agree approximately with those calculated for a uniform shear flow model (Hino et al.(5) and Andow et al.(1)). In the following sections, universal estimations on the intensities of interfacial displacements and the frequency spectra will be carried out. The discussion on phase velocities and position of critical layers will be also made.

Intensities and Spectra of Interfacial Displacements

Figs.6(a) and (b) show time series of interfacial displacements η for different values of Ri. It is found that waves with the period of about 1.5 sec are superposed on ones with the period of about 8 sec. Hereafter, we refer to the short period waves and the long period waves as 'S.P. wave' and 'L.P. wave', respectively. The S.P. wave has a steep crest and a flat trough, and conversely the L.P. wave a flat crest and a steep trough as shown in the figures.

The r.m.s. values η' of the displacements normalized by $U_*^2 / \varepsilon g$ are plotted against Ri in Fig. 7. The values of $\varepsilon g\eta'/U_*^2$ decrease with increase of Ri and are described empirically by the following equation.

$$\varepsilon g\eta'/U_*^2 = 19\, Ri^{-1/3} \qquad (6)$$

Frequency spectra $E\eta(f)$ obtained from the time series of interfacial displacements have usually two peaks of the power density. One in the lower frequency side is due to the L.P. wave and the other due to the S.P. wave (18). We try to normalize $E\eta(f)$ and frequency f on the basis of η' and the frequency f_{sp} of the most predominant S.P. wave, because the power peak of

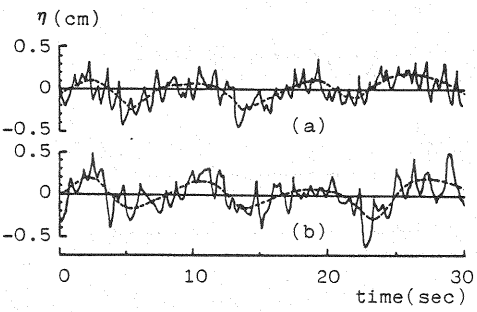

Fig. 6 Time series of interfacial displacements.

	Ri	η'(cm)	U_*(cm/s)	εg(cm/s^2)
(a)	4.93	0.137	0.556	22.3
(b)	1.15	0.216	0.336	10.6

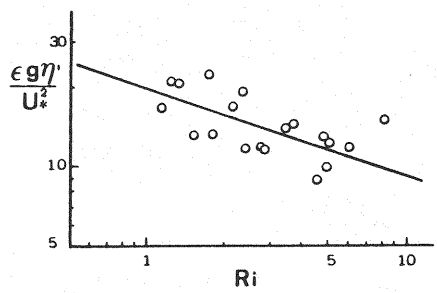

Fig. 7 Ri-dependence of $\varepsilon g\eta'/U_*^2$.

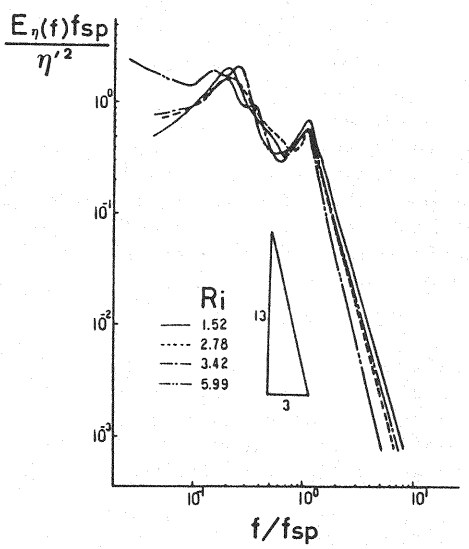

Fig. 8 Non-dimensional spectrum profiles of interfacial fluctuations.

the S.P. wave is often more distinct than that of the L.P. wave. Profiles of $E_\eta(f)f_{sp}/\eta'^2$ are shown for different values of Ri in Fig. 8. It is found that they are expressed by a universal profile. The ratio of the frequency f_{Lp} of the L.P. wave to f_{sp} is about 0.198 according to the results shown in Fig. 8 and obtained in other runs. Considering the -13/3 power-law proposed by Tsubaki et al.(18), the spectra in the equilibrium range are expressed by

$$E_\eta(f) = 2.0\eta'^2 f_{sp}^{10/3} f^{-13/3} \tag{7}$$

In Fig. 9, $f_{sp}U_*/\varepsilon g$ and f_{sp}/N are plotted against Ri, where $N=\sqrt{\varepsilon g/\delta\rho}$ = Brunt Väisälä frequency at the interface. The resulting values are

$$f_{sp}U_*/\varepsilon g = 0.0231 \quad ; \quad f_{sp}/N = 0.166 \tag{8}$$

A remark should be made on the relationship between the interfacial parameters K and Ri. The parameter Ri is rewritten as follows.

$$\begin{aligned} Ri &\equiv \frac{-g(d\rho/dy)}{\rho_2(dU/dy)^2}\Big|_{y=0} \\ &= \frac{\varepsilon g/\delta\rho}{(U_*/\delta_*)^2} = \frac{\varepsilon g\nu}{U_*^3}\frac{\nu_e}{\nu}\frac{\delta_*}{\delta\rho} = K^{-1}\frac{\nu_e}{\nu}\frac{\delta_*}{\delta\rho} \end{aligned} \tag{9}$$

By considering that ν_e and $\delta\rho$ depend on εg, ν, U_* and δ_*, we obtain the following equations from the dimensional analysis.

$$\nu_e/\nu = f_1\left(\frac{U_*^3}{\varepsilon g\nu}, \frac{U_*\delta_*}{\nu}\right)$$

$$= f_1\left(\frac{U_*^3}{\varepsilon g\nu}, \frac{\nu_e}{\nu}\right)$$

$$\delta\rho/\delta_* = f_2\left(\frac{\varepsilon g\delta_*}{U_*^2}, \frac{U_*\delta_*}{\nu}\right)$$

$$= f_3\left(Ri, \frac{\nu_e}{\nu}\right)$$

The non-dimensional quantities ν_e/ν depends on only one parameter K and that is consistent with the discussion made about Fig.4. It is found from Eq.9 and the above results that Ri and K are connected with each other, i.e.

$$Ri = f(K)$$

Therefore, estimating the dependences of the interfacial quantities on Ri is equivalent to that on K. A relationship between δ_*/δ_ρ and Ri is shown in Fig. 10. The dependence of δ_*/δ_ρ on $Ri^{1/2}$ is recognized in the present experiments. As $\nu_e/\nu \propto K^{1/2}$ in the range of large values of K, Ri is proportinal to K^{-1}

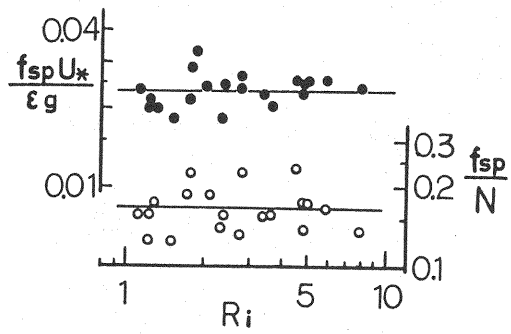

Fig. 9 Ri-dependences of $f_{sp}U_*/\varepsilon g$ and f_{sp}/N.

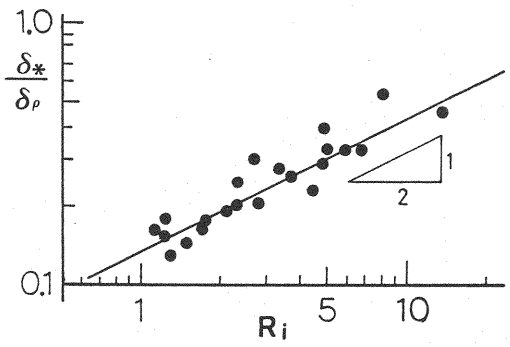

Fig. 10 Ri-dependence of δ_*/δ_ρ.

Phase Velocities, Wave Lengths and Position of Critical Layers

A dispersion relation of interfacial waves in two-layered flows with a linear velocity profile has been obtained by Hamada and Kato (3). If the frequency f is used instead of the wavenumber in the relation, phase velocities C_+ and C_- are given by

$$\frac{C_\pm}{Ui} = \left(1 + \frac{1}{8\pi}\frac{\varepsilon g}{fUi} \right) \pm \sqrt{\frac{1}{8\pi}\frac{\varepsilon g}{fUi}\left(2 + \frac{1}{8\pi}\frac{\varepsilon g}{fUi} \right)} \qquad (10)$$

$$\frac{C_\pm}{Um} = \frac{1}{2}\left[\left(1 + \frac{1}{4\pi}\frac{\varepsilon g}{fUm} \right) \pm \sqrt{\left(1 + \frac{1}{4\pi}\frac{\varepsilon g}{fUm} \right)^2 - 2} \right] \qquad (11)$$

in which it is assumed that the waves are deep water waves. Eq.10 is obtained from the uniform shear flow model which is a model of two-layered flows with fluid velocity Ui at the interface and a constant velocity gradient, and Eq.11 from a K-H wave model with a uniform velocity Um in an upper layer and with a still lower layer. The assumption of the deep water wave seems to be valid since the upper- and lower-layers have been deeper than a half length of the predominant waves according to visual observations. Phase velocities calculated from the phase lag between interfacial displacements measured at the two points are shown in Fig.11, where the solid line indicates Eq.10 and the broken line is obtained by estimating Ui/Um = 0.5 in Eq.11. The velocities of the S.P. wave are faster than Ui and those of the L.P. wave are slower. The experimental results agree well with ones for the uniform shear model rather than the K-H wave model.

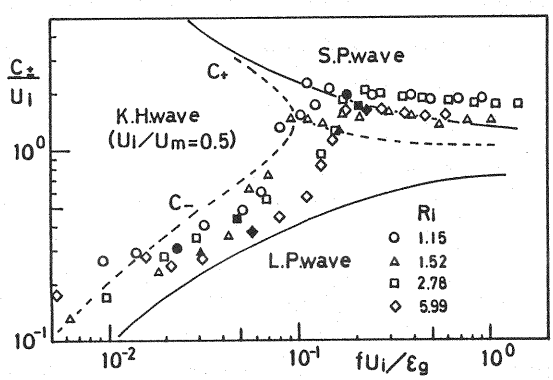

Fig. 11 Phase velocities of component waves of interfacial fluctuations. Solid symbols indicates phase velocities of the most predominant L.P. and S.P. waves.

A wave length λ_{sp} of the most predominant S.P.wave is expressed by C_{sp}/f_{sp} ; C_{sp}= phase velocity of the wave. As $f_{sp}/N = 0.166$ and $N = \sqrt{\varepsilon g/\delta_\rho}$, we obtain

$$\frac{\lambda_{sp}}{\delta_m} = \frac{C_{sp}}{Um}\frac{Um}{f_{sp}\delta_m}$$

$$= \frac{1}{0.166}\frac{C_{sp}}{Um}\frac{Um/\delta_m}{\sqrt{\varepsilon g/\delta_\rho}}$$

$$= 6.02\frac{C_{sp}}{Um}Ri^{-1/2} \qquad (12)$$

As $f_{Lp}/f_{sp} = 0.198$, λ_{Lp} is given by

$$\frac{\lambda_{Lp}}{\delta_m} = 30.4\frac{C_{Lp}}{Um}Ri^{-1/2} \qquad (13)$$

Thus, it is found that the wavelengths are proportinal to $Ri^{-1/2}$. The wavelengths derived from the measured phase velocities and frequencies are plotted against Ri in Fig.12. The wavelengths show the $Ri^{-1/2}$-dependence approximately, and that is

consistent with the results indicated by Eqs. 11 and 12.

Fig.13 shows the position of critical layers at which the mean fluid velocity coincides with the phase velocity. The phase velocities of the most predominant S.P. and L.P. waves are used as representative phase velocities. The values of y/δ_m of the critical layers are almost constant and are described by

$$y/\delta_m = 1.03 \pm 0.48 \qquad \text{for S.P. wave}$$

$$y/\delta_m = -0.27 \pm 0.12 \qquad \text{for L.P. wave}$$

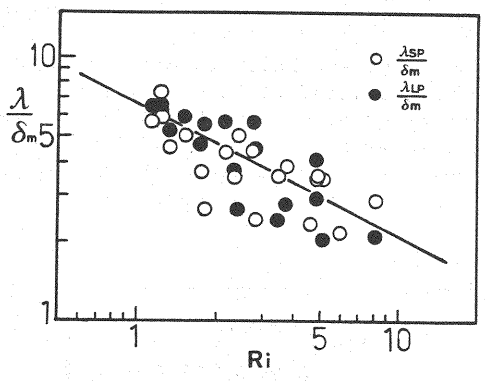

Fig. 12 Relationship between wavelengths and Ri.

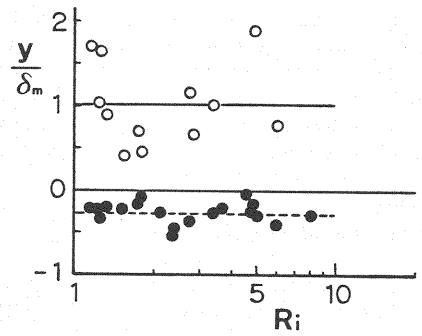

Fig. 13 Position of critical layers.

VELOCITY FLUCTUATIONS

Velocity fluctuations measured by using the velocity probe are due to turbulent shear flow, interfacial wave motion and vortical organized motion of the cat's eye pattern forming in both sides of the interface. The interfacial layer is regarded as a turbulent layer because of the irregularity of the wave motion and the organized motion. In the following sections, empirical formulae on intensities and length scales of the velocity fluctuations will be obtained, and the relationship between fluctuating velocities and interfacial displacements will be discussed.

Intensities and Length Scales of Velocity Fluctuations

Figs. 14(a) and (b) show vertical profiles of u'/U_* and v'/U_*, where u', v' = r.s.m. values of fluctuating velocities in the x- and y-directions. The profiles of u'/U_* have maximum values near the interface when $1 \lesssim Ri \lesssim 2$, and the maximum values are seen in both sides of the interface when $Ri \gtrsim 2$. The profiles of v'/U_* do not have distinct peaks in the lower layer. The maximum intensities and the intensities at the interface decrease with increase of Ri. As y/δ_m increases in the upper layer, the intensities decrease and converge to constant values in the uniform layer. In the lower layer, they decrease rapidly with decrease of y/δ_m and vanish ay $y/\delta_m \simeq -1.0$. Thus, Ri plays an important role for the fluctuating velocities.

Figs.15(a) - (d) show the dependences of the maximum, interfacial and uniform intensities on Ri. The maximum values in the upper layer, i.e. $(u'/U_*)_{max}^{upper}$ and $(v'/U_*)_{max}^{upper}$, are shown in Fig.15(a). They are proportional to $Ri^{-1/3}$. The interfacial intensities $(u'/U_*)_{y=0}$ and $(v'/U_*)_{y=0}$ are proportional to $Ri^{-2/3}$ as

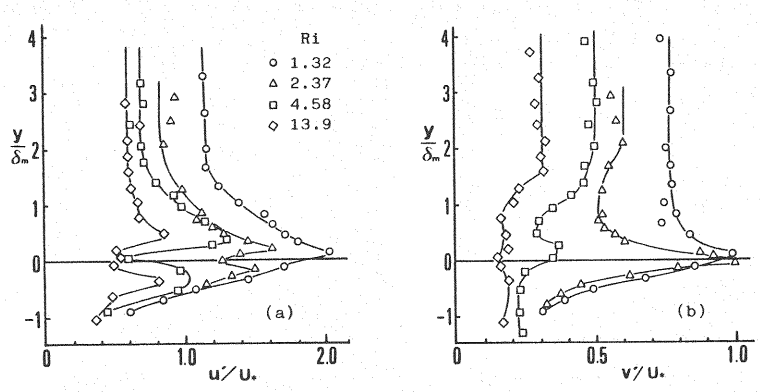

Fig. 14 Vertical profiles of intensities of fluctuating velocities.

shown in Fig.15(b). Fig.15(c) shows that the maximum values $(u'/U_*)^{lower}_{max}$ in the lower layer have the approximately same Ri-dependence as those in the upper layer. It is found that the Ri-dependences of $(u'/U_*)_{y=0}$ and $(v'/U_*)_{y=0}$ are stronger than that of the maximum intensities. The intensities $(u'/U_*)_{uniform}$ in the uniform layer which is in the range of $y \gtrsim h_1' \approx 2.1\ \delta_m$ are almost constant as shown in Fig. 15(d). The ratio of $(u'/U_*)_{uniform}$ to $(v'/U_*)_{uniform}$ is about 1.8 . Fig.16

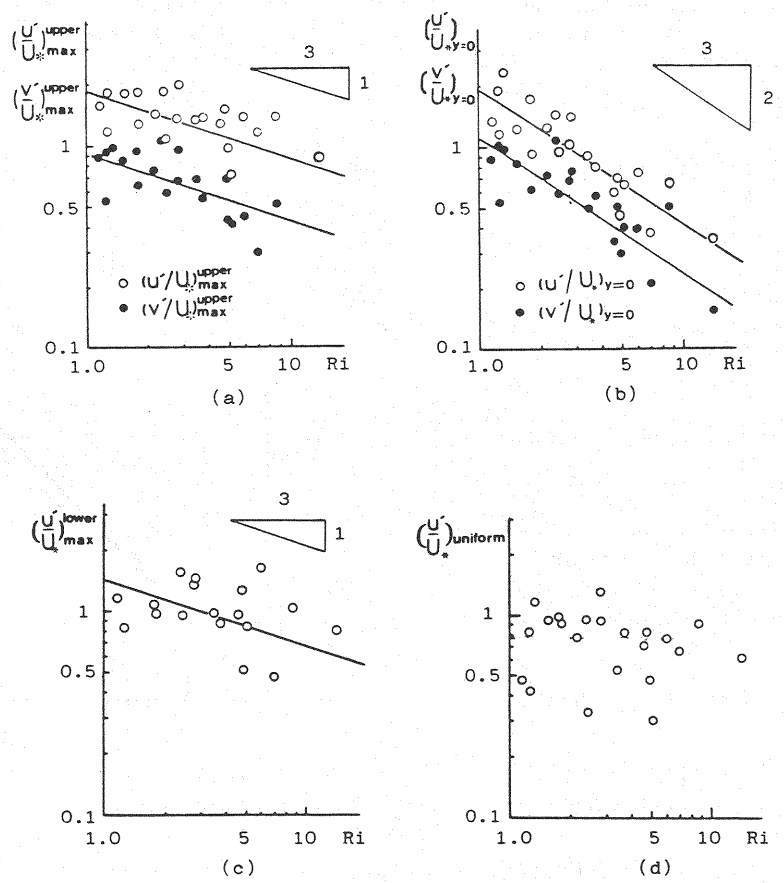

Fig. 15 Ri-dependences of intensities of fluctuating velocities.

shows the positions y/δ_m of the maximum intensities against Ri. They are given by

$$\left(\frac{y}{\delta_m}\right)^{upper}_{u'max} = \begin{cases} 0.17 \pm 0.07 & (Ri \lesssim 3.5) \\ 0.46 \pm 0.24 & (Ri \gtrsim 3.5) \end{cases} \qquad (14)$$

$$\left(\frac{y}{\delta_m}\right)^{upper}_{v'max} = 0.13 \pm 0.09$$

$$\left(\frac{y}{\delta_m}\right)^{lower}_{u'max} = -0.32 \pm 0.19$$

where e.g. $(y/\delta_m)^{upper}_{u'max}$ indicates the non-dimensional position of the maximum value of u' in the upper layer. Considering that the position $(y/\delta_m)^{lower}_{u'max}$ agrees well with the position of the critical layers in the lower layer, we find that the velocity fluctuations in the lower layer are induced by the organized vortical motion of the cat's eye pattern.

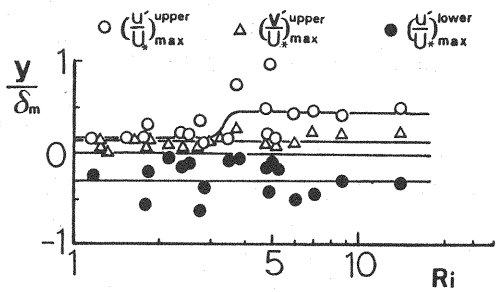

Fig. 16 Ri-dependences of positions of the maximum intensities.

We discuss about the fluctuating velocities induced by the wave motion. When a wave of which the profile is described by

$$\eta = a \cos k(x - Ct)$$

exists at an interface, the equation of horizontal fluid velocity induced by the wave motion becomes

$$u_j = (-1)^j k a (C - U_i)\, e^{(-1)^j ky} \cos k(x - Ct)$$

by using the uniform shear model; a = wave amplitude and the subscripts j=1 and 2 denote upper and lower layers, respectively. At y=0, the r.m.s. value u'_w is given by

$$u'_w = \sqrt{2}\,\pi a (C_{sp} - Ui)/\lambda_{sp}$$

where $C = C_{sp}$ and $k = 2\pi/\lambda_{sp}$ are used. Moreover, considering that the frequency distribution of interfacial wave heights obeys a Rayleigh distribution (12), we obtain $a = 1.25\,\eta'$. Therefore, the above equation becomes

$$u_w' = 5.55\,\eta' (C_{sp} - Ui)/\lambda_{sp}$$

The relationship between u'_w calculated on the basis of the measured values of η', Ui, C_{sp} and λ_{sp} and the measured values of $u'_{y=0}$ is shown in Fig.17. It is found that $u'_{y=0} \approx u'_w$ and the velocity fluctuations near the

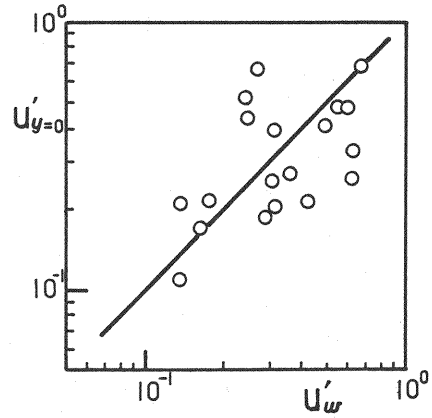

Fig. 17 Relationship between $u'_{y=0}$ and u'_w.

interface is generated mainly by the wave motion. The scatter of the data may be due to the use of only the quantities related to the most predominant S.P. wave.

Integral length scales Lx of the velocity fluctuations are estimated by the equation,

$$Lx = U(y)\,T = U(y)\,E_u(0)/\,4u'^2$$

where $T = E_u(0)/4u'^2$ = integral time scale of the velocity fluctuation u ; and $E_u(f)$ = frequency spectrum of u. As shown in Fig.18, the vertical distribution of Lx is given by

$$\frac{Lx}{\delta_m} = 1 + \frac{y}{\delta_m} \quad \left(-1 \lesssim \frac{y}{\delta_m} \lesssim \frac{h_1}{\delta_m} \simeq 2.1\right)$$

$$\frac{Lx}{\delta_m} = 3.1 \quad \left(2.1 \lesssim \frac{y}{\delta_m}\right) \qquad (15)$$

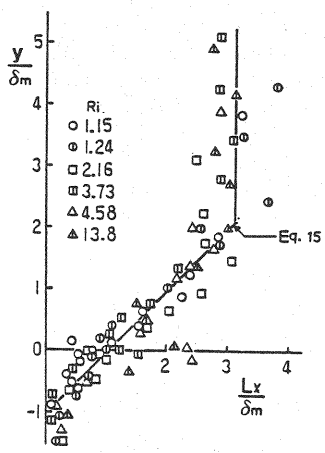

Fig. 18 Vertical distribution of integral length scales.

Spectra of Velocity Fluctuations

Figs.19(a) and (b) show frequency spectra $E_u(f)$ and $E_v(f)$ of the fluctuating velocities measured at y = 0.68 cm and 3.32 cm, and $E_\eta(f)$. It is found that near the interface $E_u(f)$ and $E_v(f)$ have peaks of the power density at the frequencies equal to those of the S.P. and L.P. waves. The inertial subrange proportional to $f^{-5/3}$ is not seen owing to the influence of the S.P. wave, but the -13/3 power-law of f, which is proposed by Tsubaki and Komatsu (17), holds in the viscous subrange. In $E_u(f)$ at y = 3.32 cm, the inertial subrange forms without disturbed by the S.P. wave though the influence of the L.P. wave remains yet. The influence of the S.P. wave on $E_v(f)$ seems to be stronger than that of the L.P. wave at y = 3.32 cm.

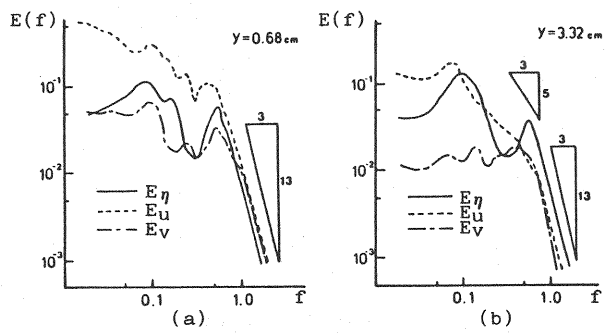

Fig. 19 Power spectra of fluctuating velocities and interfacial displacements.

In order to transform $E_u(f)$ into a normalized form of one-dimensional wavenumber spectrum F(k), $E_u(f)$ and f are non-dimensionalized as follows:

$$F^*(k^*) = \frac{U(y)\,E_u(f)}{2\pi\,Lx\,u'^2} = \frac{E_u(f)}{2\pi u'^2\,T} \qquad (16)$$

$$k^* = Lx\,k = 2\pi\,T\,f$$

where k = wavenumber and the asterisk denotes a non-dimensional quantity. Fig.20 shows $F^*(k^*)$ for the different values of y/δ_m. The broken line indicates the equation

$$F^*(k^*) = \frac{2}{\pi}\left(1 + k^{*2}\right)^{-5/6} \qquad (17)$$

which has been proposed as a reasonable equation for the productive and inertial subranges of homogeneous, isotropic turbulence by Kármán (8). The spectra $F^*(k^*)$ in the upper-layer flow agree with Eq. 17 basically, though near the interface they have peakes of the power at the wavenumber corresponding to those of the S.P. and L.P. waves. In the viscous subrange, a reasonable equation

$$F(k) \propto \nu^{-2} \left(\frac{u'^3}{Lx}\right)^{4/3} k^{-13/3}$$

has been proposed (17), and it is normalized as follows.

$$F^*(k^*) \propto k^{*-13/3} \left(\frac{u'Lx}{\nu}\right)^2 \qquad (18)$$

Therefore, the scattering of $F^*(k^*)$ in the viscous subrange may depend on the Reynolds number of turbulent eddies.

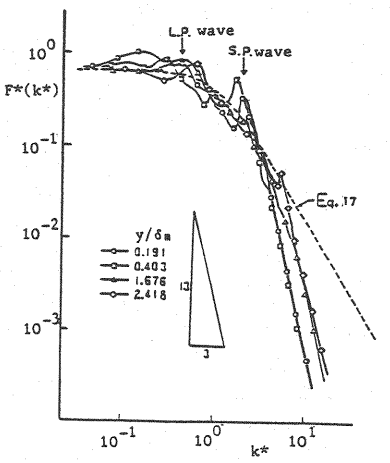

Fig. 20 Normalized wavenumber spectra of fluctuating velocities.

INTERFACIAL FRICTION COEFFICIENT

The coefficient f_i of interfacial friction is defined by

$$f_i = 2 \left(U_* / Um \right)^2$$

As shown in Fig. 21, numerous experimental results have indicated that f_i depends on Ψ though they are scattered. An empirical formula proposed by Kaneko (7),

$$f_i = 0.2\, \Psi^{-1/2} \qquad (19)$$

has been supported as the best to fit the experimental results. The present

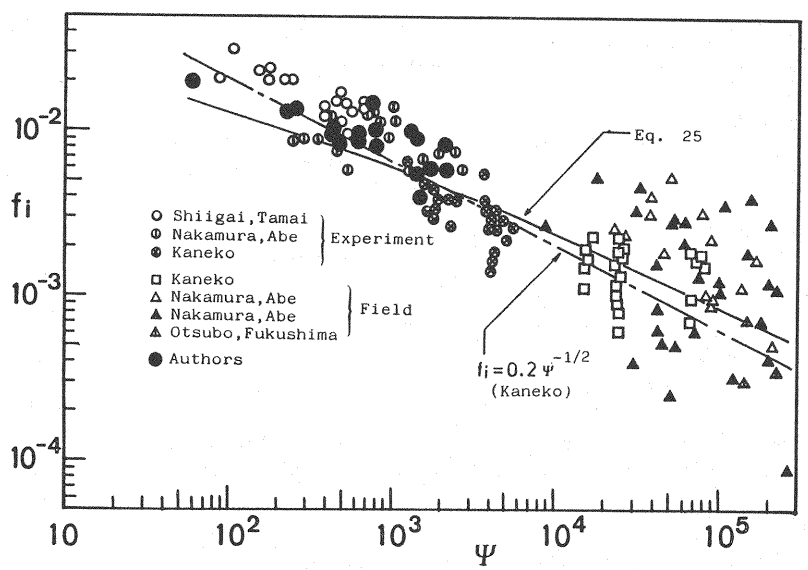

Fig. 21 Relationship between f_i and Ψ.

experimental results are also plotted in the figure and the data fit approximately to Eq. 19.

We try to estimate f_i by analyzing the velocity profile in the lower layer on the basis of the above-mentioned experimental results and satisfying the continuity of the mean velocity at the interface. First, velocity profiles in the interfacial layer ($0 \geqq y \geqq -\Delta_2$) of the lower layer and the quasi-viscous layer ($-\Delta_2 \geqq y \geqq -h_2'$) will be discussed. The intensities u' increase with decrease of y in the lower layer, and diminish rapidly with decrease of y after it has a maximum value (see Fig. 14). Here, Δ_2 is defined as the distance from the interface to the position at which u' takes a maximum value in the lower layer. Considering these results, we assume a vertical distribution of an effective viscosity ν_e' in the lower layer, i.e. ν_e' takes ν_e, $\gamma\nu_e$ and ν at y=0, $-\Delta_2$ and $-h_2'$, respectively, increases linearly in the range of $0 \geqq y \geqq -\Delta_2$, and decreases parabolically in the range of $-\Delta_2 \geqq y \geqq -h_2'$, where γ = a constant value determined empirically. The distribution of ν_e' is shown schematically in Fig.22. It is expressed by

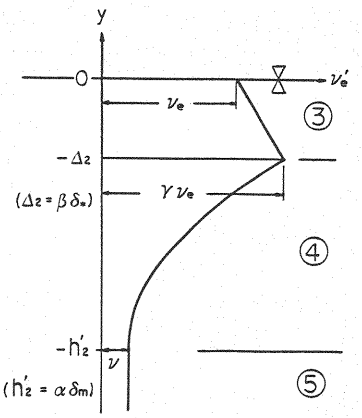

Fig. 22 Distribution of ν_e'.
③ interfacial layer,
④ quasi-viscous layer,
⑤ return flow layer.

$$\nu_e' = \nu_e \left[1 - \frac{\phi_m}{\beta} (\gamma - 1) \frac{y}{\delta_m} \right] \qquad \text{for} \quad 0 \geqq y \geqq -\Delta_2$$

$$\nu_e' = \nu + \frac{\gamma\nu_e - \nu}{\left(\frac{\beta}{\phi_m} - \alpha \right)^2} \left(\frac{y}{\delta_m} + \alpha \right)^2 \qquad \text{for} \quad -\Delta_2 \geqq y \geqq -h_2'$$

using $\beta = \Delta_2/\delta_*$, $\alpha = h_2'/\delta_m$ and $\phi_m = U_m/U_* = \delta_m/\delta_*$.

The distribution of shear stress τ is assumed generally to be a linear profile as given by

$$\frac{\tau}{\rho_2} = \nu_e' \frac{dU}{dy} = U_*^2 \left(1 + \frac{y}{h_2'} \right) \tag{20}$$

By integrating Eq. 20 and using $U = U_i$ at $y = 0$ and $U = 0$ at $y = -h_2'$ as boundary conditions, the equations

$$-\beta/\phi_m \leqq y/\delta_m \leqq 0 \ ;$$

$$\frac{U_i - U}{U_*} = \frac{\beta}{\alpha(\gamma - 1)} \frac{y}{\delta_m} + \frac{\beta^2}{\phi_m(\gamma - 1)^2} \left\{ \frac{\phi_m}{\beta}(\gamma - 1) + \frac{1}{\alpha} \right\} \times \ln \left[1 - \frac{\phi_m}{\beta}(\gamma - 1) \frac{y}{\delta_m} \right]$$

$$-\alpha \leqq y/\delta_m \leqq -\beta/\phi_m \ ; \tag{21}$$

$$\frac{U_i - U}{U_*} = \frac{U_i - U_{-\Delta_2}}{U_*} + \frac{\nu_e}{\nu} \frac{\phi_m (\alpha - \beta/\phi_m)^2}{2\alpha\left(\gamma\frac{\nu_e}{\nu} - 1\right)} \times \ln \left[\frac{\gamma\frac{\nu_e}{\nu}}{\left(\gamma\frac{\nu_e}{\nu} - 1\right)\left(\frac{\alpha + y/\delta_m}{\alpha - \beta/\phi_m}\right)^2 + 1} \right]$$

are derived, where $U_{-\Delta_2}$ = mean velocity at $y = -\Delta_2$.

The following equation for U_i is obtained from the continuous condition of fluid velocity at $y/\delta_m = -\beta/\phi_m$.

$$\frac{U_i}{U_*} = \frac{\nu_e}{\nu}\frac{\phi_m(\alpha-\beta/\phi_m)^2}{2\alpha(\gamma\frac{\nu_e}{\nu}-1)}\ln(\gamma\frac{\nu_e}{\nu}) + \frac{\beta^2}{\phi_m(\gamma-1)}\times\left[-\frac{1}{\alpha}+\left\{\frac{\phi_m}{\beta}+\frac{1}{\alpha(\gamma-1)}\right\}\ln\gamma\right] \quad (22)$$

If a condition of $U = U_1$ at $y = h_1'$ is applied to Eq.4 ,

$$\phi_m\frac{U_1}{U_m} = \frac{U_i}{U_*} + \frac{U_*\Delta_1}{\nu_e} + 2.5\ln\left(\phi_m\frac{h_1'}{\delta_m}\Big/\frac{U_*\Delta_1}{\nu_e}\right) \quad (23)$$

is obtained.

Second, the experimental results are considered. Averaged values and standard deviations of α, β and U_1/U_m are given by

$$\alpha = \frac{h_2'}{\delta_m} = 1.13 \pm 0.2$$

$$\beta = \frac{\Delta_2}{\delta_*} = 5.0$$

$$\frac{U_1}{U_m} = 1.08 \pm 0.026$$

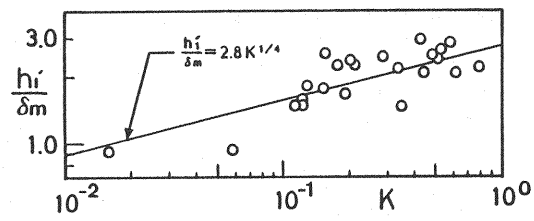

Fig.23 K-dependence of h_1'/δ_m.

Fig.23 shows h_1'/δ_m plotted against K. From the figure, the equation

$$\frac{h_1'}{\delta_m} = 2.8\,K^{1/4} = 2.8(\Psi\,\phi_m^{-3})^{1/4} \quad (24)$$

is obtained. Substituting Eqs. 22 and 24 into Eq.23 , we obtain

$$\phi_m\frac{U_1}{U_m} = \frac{\nu_e}{\nu}\frac{\phi_m(\alpha-\beta/\phi_m)^2}{2\alpha(\gamma\,\nu_e/\nu-1)}\ln(\gamma\frac{\nu_e}{\nu}) + \frac{\beta^2}{\phi_m(\gamma-1)}\left[-\frac{1}{\alpha}+\left\{\frac{\phi_m}{\beta}+\frac{1}{\alpha(\gamma-1)}\right\}\times\ln\gamma\right] + \frac{U_*\Delta_1}{\nu_e} + 2.5\ln\left[2.8(\Psi\,\phi_m)^{1/4}\Big/\frac{U_*\Delta_1}{\nu_e}\right] \quad (25)$$

In order to determine the value of γ , the relationship at $y = -\Delta_2$ derived from the first equation of Eq.21 is used. Considering the experimental results that $(U_i - U_{-\Delta_2})/U_* \simeq -3.7$ at $y = -\Delta_2 = -5.0\,\delta_*$ according to Fig.5 and the mean value of ϕ_m is about 15.4 , we obtain $\gamma = 1.33$.

By using experimental constant values for U_1/U_m , α , $U_*\Delta_1/\nu_e$ ($\simeq 4.0$), β and γ, the empirical equation $\nu_e/\nu = (1+40K)^{1/2} = [1+40(\Psi\,\phi_m^{-3})]^{1/2}$ (see Eq.2) and $\phi_m \simeq \sqrt{2/f_i}$, f_i can be expressed as a function of the single parameter Ψ . The calculated results are shown by a solid line in Fig. 21. Though numerous parameters are included in this theory and are determined experimentally, the results agree well with ones obtained in both experimental studies and field observations.

CONCLUSIONS

The conclusions obtained in this experimental study are as follows:

1. A universal profile of the mean velocity in upper layer is indicated Eqs. 3, 4 and 5, when the effective viscosity is used.

2. The interfacial fluctuations consist of the S.P. wave and the L.P. wave, and a universal profile of non-dimensional spectra of the fluctuations is obtained when spectra are normalized by using intensities of interfacial displacements and predominant frequencies of the S.P. wave. The ratio of the distance from the interface to critical layers to δ_m is almost constant.

3. The vertical profiles of u'/U_* have maximum values usually in both sides of the interface. The maximum values are proportional to $Ri^{-1/3}$ and interfacial values to $Ri^{-2/3}$. The velocity fluctuations in the interfacial layer are induced by the wave motion and the vortical organized motion of the cat's eye pattern. Non-dimensional integral length-scales of the velocity fluctuations are given by Eq. 15.

4. A simulation model has been proposed on the basis of the experimental results in order to estimate the coefficient of interfacial friction. The results obtained by using the model agree well with ones measured in both experimental studies and field observations.

It is considered that additional experiments should be carried out in a wide range of Ri or K in order to obtain more accurate estimations.

The authors thank Dr T. Komatsu for stimulating discussions and T. Shibata, T. Namikawa and T. Koga for technical help.

REFERENCES

1. Andow, T., K. Hanawa and Y. Toba : Experimental study on internal waves in a stratified shear flow, J. Oceanogr. Soc. Japan, Vol.37, pp.179-192, 1981.
2. Csanady, G.T. : Turbulent interface layer, J. Geophys. Res., Vol.83, pp.2329-2342, 1978.
3. Hamada, T. and H. Kato : Two-layered flows and internal waves, Proc. 9th Japanese Conf. on Coastal Eng., JSCE, pp.61-63, 1962. (in Japanese).
4. Hino, M. and K. Hagiwara : On applicability of the Monin-Obukhov theory of the velocity distribution of saltwedge, Proc. 26th Japanese Conf. on Coastal Eng., JSCE, pp.549-553, 1979. (in Japanese).
5. Hino, M., S.H. Nguyen and K. Nakamura : Interfacial friction and flow structure of two-layered stratified flows, Proc. 28th Japanese Conf. on Coastal Eng., JSCE, pp.515-519, 1981. (in Japanese).
6. Hino, M. and S.H. Nguyen : Velocity distribution, interfacial friction and entrainment in two-layered stratified flows, J. Hydrosci. and Hydr. Eng., Vol. 1, No.1, pp.9-36, 1983.
7. Kaneko, Y. : An example of the interfacial drag coefficient of two-layered flows, Proc. 16th Japanese Conf. on Coastal Eng., JSCE, pp.263-267, 1966. (in Japanese).
8. Karman, T. : Progress in the statistical theory of turbulence, Proc. Nat. Acad. Sci. U.S., Vol.34, pp.530-539, 1948.
9. Kato, H. and T. Ikeda : Experiment on stratified lower-layer flow (1), Proc. 28th Japanese Conf. on Coastal Eng., JSCE, pp.520-524, 1981. (in Japanese).
10. Kato, H., S. Nakano and T. Ikeda : Experiments on stratified lower-layer flow (2) - entrainment, internal wave and turbulent characteristics -, Proc. 29th Japanese Conf. on Coastal Eng., JSCE, pp.540-544, 1982. (in Japanese).

11. Keulegan, G.H. : Interfacial instability and mixing in stratified flow, J. of Res., Nat. Bur. Stand., Vol.43, pp.487-500, 1949.
12. Komatsu, T., M. Imasaka and T. Tsubaki : Statistical properties of internal waves at the interface of two-layered flow, Tech. Rep. Kyushu Univ., Vol.52, No.1, pp.25-32, 1979. (in Japanese).
13. Lofquist, K. : Flow and stress near interface between stratified liquids, Phys. Fluids, Vol.3, pp.158-175, 1960.
14. Murota, A. and T. Hirata : On internal wave behavior and mixing mechanism at interface of two-layered flow, Proc. 22nd Japanese Conf. Hydr., JSCE, pp.107-112, 1978. (in Japanese).
15. Nishida, S. and S. Yoshida : Stability analysis on two-layered flow, Proc. 29th Japanese Conf. on Coastal Eng., JSCE, pp.550-554, 1982. (in Japanese).
16. Tsubaki, T., H. Hamamura and M. Hashimoto : On the statistical properties of internal waves formed at the interface of arrested saline wedge, Proc. 13th Cong. I.A.H.R., Vol.3, pp.157-164, 1969.
17. Tsubaki, T. and T. Komatsu : Spectral properties of turbulence and density fluctuation in a stratified shear flow, Proc. JSCE, No.268, pp.63-74, 1977. (in Japanese).
18. Tsubaki, T., T. Komatsu and G. Shimoda : Experimental study on interfacial wave and turbulence of two-layered flow, Proc. 25th Japanese Conf. on Hydr., JSCE, pp.311-319, 1981. (in Japanese).
19. Yoshida, S : On a mechanism for mixing across density interface, Proc. JSCE, No.273, pp.59-68, 1978. (in Japanese).

APPENDIX - NOTATION

The following symbols are used in this paper:

a = amplitude of an interfacial wave;

B = width of the experimental flume;

C = phase velocity of the interfacial wave;

C_{LP}, C_{SP} = phase velocities of the most predominant L.P. and S.P. waves;

$(dU/dy)_{y=0}$ = gradient of the mean velocity at the interface;

$(d\rho/dy)_{y=0}$ = gradient of the mean density at the interface;

$E_u(f)$, $E_v(f)$ = frequency spectra of the velocity fluctuations u and v;

$E_\eta(f)$ = frequency spectrum of the interfacial fluctuations η;

f = frequency;

f_i = interfacial friction coefficient;

f_{LP}, f_{SP} = frequencies of the most predominant L.P. and S.P. waves;

$F(k)$, $F^*(k^*)$ = wavenumber spectrum and non-dimensional wavenumber spectrum of the velocity fluctuations;

Fr = internal Froude number;

g = acceleration of gravity;

h = water depth;

h_1, h_2 = mean depths of the upper and lower layers;

h_1', h_2' = distances from $y=0$ to the position of $U(y)=U_1$ and to the position of $U(y)=0$;

k, k^* = wavenumber and non-dimensional wavenumber;

K = interfacial Keulegan parameter;

Lx = integral length scale of the velocity fluctuations;

N = Brunt-Väisälä frequency at the interface;

Re = Reynolds number;

Ri = interfacial Richardson number;

t = time;

T = integral time scale of the velocity fluctuations;

u, v = fluctuating velocities along x and y;

u', v' = r.m.s. values of the fluctuating velocities;

u'_w = r.m.s. value of the velocity induced at the interface by a wave;

U_i = mean velocity at the interface;

U_m = velocity averaged in the cross-section of an upper layer;

U_* = interfacial shear velocity;

U_1 = mean velocity in the uniform flow layer;

$U(y)$ = mean velocity at a level y;

x, y = coordinates;

α, β = ratios of characteristic lengths as defined by h_2'/δ_m and Δ_2/δ_*;

γ = increasing rate of ν_e in the interfacial layer of a lower layer;

δ_m, δ_ρ, δ_* = Length scales as defined by $U_m/(dU/dy)_{y=0}$, $(\rho_2-\rho_1)/|d\rho/dy|_{y=0}$ and $U_*/(dU/dy)_{y=0}$;

Δ_1, Δ_2 = thicknesses of the interfacial layer in upper and lower layers;

ϵ = non-dimensional density differrence as defined by $(\rho_2-\rho_1)/\rho_2$;

η, η' = interfacial displacement and r.m.s. value of it;

κ = von Karman constant;

λ_{LP}, λ_{SP} = wavelengths of the L.P. and S.P. waves;

ν, ν_e = kinematic viscosity and effective viscosity;

ρ_1, ρ_2 = mean densities of the upper and lower layers;

$\rho(y)$ = mean density at a level y;

τ_w = shear stress acting on a side wall;

ϕ_m = U_m/U_* = velocity coefficient; and

Ψ = Iwasaki number.